Terahertz Emission Increase in GaAs Films Exhibiting Structural Defects Grown on Si (100) Substrates Using a Two-Layered LTG-GaAs Buffer System

Karl Cedric Gonzales
Universitat Jaume I

Elizabeth Ann Prieto (eapprieto@msep.upd.edu.ph)
University of the Philippines Diliman https://orcid.org/0000-0002-0255-2605

Gerald Angelo Catindig
University of the Philippines Diliman

Alexander De Los Reyes
University of the Philippines Diliman

Maria Angela Faustino
University of the Philippines Diliman

Mae Agatha Tumanguil-Quitoras
University of the Philippines Diliman

Horace Andrew Husay
University of the Philippines Diliman

John Daniel Vasquez
University of the Philippines Diliman

Armando Somintac
University of the Philippines Diliman

Elmer Estacio
University of the Philippines Diliman

Arnel Salvador
University of the Philippines Diliman

Research Article

Keywords: Molecular Beam Epitaxy, Gallium Arsenide, Silicon, III-V Semiconductor Devices, Terahertz Devices

Posted Date: February 18th, 2021

DOI: https://doi.org/10.21203/rs.3.rs-207583/v1

Version of Record: A version of this preprint was published at Journal of Materials Science: Materials in Electronics on April 22nd, 2021. See the published version at https://doi.org/10.1007/s10854-021-05958-8.

Abstract

Terahertz (THz) emission increase is observed for GaAs thin films that exhibit structural defects. The GaAs epilayers are grown by molecular beam epitaxy on exactly oriented Si (100) substrates at three different temperatures (T_s = 320ºC, 520ºC and 630ºC). The growth method involves the deposition of two low-temperature-grown (LTG)-GaAs buffers with subsequent in-situ thermal annealing at T_s = 600ºC. Reflection high energy electron diffraction confirms the layer-by-layer growth mode of the GaAs on Si. X-ray diffraction shows the improvement in crystallinity as growth temperature is increased. The THz time-domain spectroscopy is performed in reflection and transmission excitation geometries. At T_s = 320ºC, the low crystallinity of GaAs on Si makes it an inferior THz emitter in reflection geometry, over a GaAs grown at the same temperature on a semi-insulating GaAs substrate. However, in transmission geometry, the GaAs on Si exhibits less absorption losses. At higher T_s, the GaAs on Si thin films emerge as promising THz emitters despite the presence of antiphase boundaries and threading dislocations as identified from scanning electron microscopy and Raman spectroscopy. An intense THz emission in reflection and transmission excitation geometries is observed for the GaAs on Si grown at T_s = 520ºC, suggesting the existence of an optimal growth temperature for GaAs on Si at which the THz emission is most efficient in both excitation geometries. The results are significant in the growth design and fabrication of GaAs on Si material system intended for future THz photoconductive antenna emitter devices.

Relevance Summary

- Demonstration of GaAs integration on exact n-type undoped Si(100) by MBE using a two-layer LTG-GaAs buffer system. The buffer system allows for a controlled growth of relatively high-quality GaAs layers at different substrate temperatures as confirmed by in-situ RHEED, SEM, XRD diffraction and Raman spectroscopy.
- Utilization of Si substrates, which has a lower absorption in the THz region, to establish a GaAs-based THz emitter that is more effective in both reflection and transmission excitation geometries. The GaAs on Si material system will constitute a cost-effective THz photoconductive antenna device and likewise provide an improved refractive index matching with a Si lens mount.
- Confirmation of THz emission enhancement in GaAs on Si heterostructure, which is not solely dependent on high crystallinity but also on the presence of structural defects such as APBs.
- Validation of the reduced THz absorption losses in GaAs on Si structures advantageous for THz measurements in transmission excitation geometry.
- Establishment of GaAs on Si as a more effective material system even with the presence of structural defects over LTG-GaAs homostructure in the generation of THz radiation in both reflection and transmission excitation geometries.

Introduction

Gallium Arsenide on Silicon (GaAs on Si) is a promising semiconductor thin film for terahertz (THz) photoconductive antenna (PCA) emitters. GaAs on Si has been shown to exhibit enhanced THz emission relative to GaAs bulk wafers [1, 2]. The enhancement is associated with the strain field at the GaAs/Si interface. Fittingly, commercially available PCA emitters utilize Si lens, which is mounted at the substrate-side of the wafer to effectively collimate the outgoing THz radiation. Since most semiconductor substrates for THz PCA are GaAs-based, the refractive index mismatch between the GaAs substrate and the Si lens can cause interference distortions in the outgoing THz radiation pattern [3]. By utilizing Si as the substrate for the THz PCA, there is a near-perfect index matching with the Si lens. Thus, it is highly desirable for a GaAs to be integrated with a Si substrate for a more efficient and cost-effective THz PCA emitter.

In over three decades, the challenges in the heteroepitaxy of GaAs on Si by molecular beam epitaxy with high crystal quality have been well identified [4–9]. The difference in the lattice constant and thermal expansion coefficient between GaAs and Si result in threading dislocations, nucleation of cracks, pinholes, and generally limit the thickness of the GaAs epilayer [4–9]. Furthermore, GaAs being polar and Si being nonpolar lead to antiphase boundaries (APBs) [4–6, 8]. Several growth methods have already been reported in order to achieve GaAs on Si with high crystallinity [5–12]. Nevertheless, high crystallinity is not an exclusive requisite for intense THz emission. Semiconductors with surface structures have been shown to emit enhanced THz radiation [13, 14]. Recently, GaAs microstructures on Si has been shown to exhibit intense THz radiation in comparison with semi-insulating (SI)-GaAs [14]. The increase is attributed to the enhanced surface field in the GaAs microstructures. Although previous works have shown that both the surface [14] and interface field [1, 2] play a significant role in the enhancement of THz radiation in GaAs on Si, their growth schematics are not intended for THz PCA device fabrication. The device fabrication of PCA involves the deposition of metal contacts on a relatively smooth (specular) and thick (~ 2 μm) semiconductor epilayer [3, 15, 16]. These particularities can be challenging with the deposition of GaAs on Si.

In this work, an n-type undoped Si (100) substrate is used primarily because of the APBs dominantly present in GaAs film grown on exact Si (100) substrate [4, 5, 8, 11, 17]. A Si (100) surface has monoatomic-height steps, which favor Ga-Ga and As-As bonding upon deposition of GaAs [8]. Such bonds form boundaries identified as APBs. Structural defects such as the APBs in GaAs on Si (100) propagating in the entirety of the GaAs epilayer may prove advantageous in the emission of THz radiation by increasing the surface field. Furthermore, Si substrate has low absorption coefficient in the THz frequency region [18–20]. The work aims to establish a GaAs-based THz emitter that is more effective in both reflection and transmission THz excitation geometries. Likewise, a GaAs on Si material system will constitute a cost-effective THz PCA device and provide an improved refractive index matching with a Si lens mount.

Additionally, a two-layered, low-temperature-grown (LTG)-GaAs buffer accompanied with subsequent in-situ thermal annealing are implemented. An illustration of the growth method is shown in Fig. 1, which is designed to address the issues with the lattice mismatch and the thermal expansion coefficient

difference between GaAs and Si, at the same time, provide a simple approach in varying the APB sizes. The method is a combination of the two-step growth and the concept of utilizing an intermediate layer that are conventional in GaAs on Si processes [5–7, 9–12]. An LTG-GaAs (T_s < 450ºC [21, 22]) is a common material for the generation and detection of THz radiation by ultrafast switching of PCA [3, 15, 16]. The growth method is intended not to deviate far from the standard LTG-GaAs on SI-GaAs processes for direct comparison while establishing a ~ 2 µm-GaAs epilayer without surface cracks, pinholes and has minimized surface roughness. The deposition of GaAs on Si is performed at different substrate temperatures (T_s = 320ºC, 520ºC, 630ºC). The THz emission intensity is compared with GaAs deposited on SI-GaAs at T_s = 320ºC. There are two optical excitation geometries used for the THz emission analysis of the samples. A THz time-domain spectroscopy is performed in both reflection and transmission excitation geometries [1, 23].

Experimental Details

The GaAs epilayers were deposited on Si and SI-GaAs substrates using a Riber 32P molecular beam epitaxy (MBE). For reference, the samples were labeled according to the substrate type and the substrate temperature during the GaAs active layer deposition. Samples 320Si, 520Si, 630Si were the GaAs grown on Si (100) substrates at T_s = 320ºC, 520ºC, 630ºC, respectively, while sample 320GaAs was the GaAs grown on SI-GaAs (100) substrate at T_s = 320ºC. The epiready Si substrates (resistivity ~ 1.0 KΩ.cm), which were n-type undoped Si (100) from MTI Korea underwent successive ionic clean, oxide strip, and another ionic clean prior to MBE deposition. The ionic clean involved the submersion of the Si substrate in an HCl:H_2O_2: deionized H_2O (3:3:5) solution for 2 minutes, depositing a volatile chemical oxide to bury carbon and other contaminants on the surface. The oxide layer that formed, together with the buried contaminants, was then stripped by submerging the Si substrate in an HF:deionized H_2O (1:7) solution for 2 minutes. This oxide strip process was repeated three times before another ionic clean was carried out. A passivating layer was expected to be formed after the final ionic clean. This layer was removed inside the MBE growth chamber by heating the Si substrate at T_s = 700ºC for 10 minutes without any exposure to Ga and As beams.

The growth schematic of the samples with the nomimal thickness of each layer are shown in Fig. 2. The Ga and As used were both solid sources with the latter being a high purity 7N5 As_4. For the GaAs on Si samples, the exposure of the Si substrate to As beam commenced after T_s was lowered from T_s = 700ºC to T_s = 500ºC. When T_s was further lowered to 250ºC (320ºC) for the 320Si (520Si and 630Si) sample, the Ga beam shutter was turned on and off for 50 seconds before exposing the Si substrate on simultaneous Ga and As beams. Consequently, the first LTG-GaAs buffer was deposited at a growth rate of at least 0.2 µm/hr. The T_s, after closing the Ga beam shutter, was then raised to T_s = 600ºC for a 10-minute in-situ annealing. This was then followed by a 1.0 µm/hr deposition of the second LTG-GaAs buffer at T_s = 320ºC (420ºC) for the 320Si (520Si and 630Si) sample. The deposition of the second LTG-GaAs buffer in sample 320Si was terminated only after reaching a nominal 2µm thickness. The second

LTG-GaAs buffer was subsequently annealed at T_s = 600ºC for 10 minutes, again with a closed Ga beam shutter. After the second annealing, a 2 µm-GaAs was deposited at T_s = 520ºC and T_s = 630ºC for samples 520Si and 630Si, respectively, with a 1.0 µm/hr growth rate. Finally, a silicon-doped GaAs (n-GaAs) cap was deposited at T_s = 630ºC for all three samples intended for future PCA device fabrication. For comparison, sample 320GaAs was grown on an epiready SI-GaAs substrate (resistivity ~ 10.0 MΩ.cm). A conventional GaAs buffer deposited at T_s = 630ºC was used followed by the deposition of an LTG-GaAs at T_s = 320ºC. The LTG-GaAs was annealed at T_s = 600ºC for 10 minutes without exposure to the Ga beam. The deposition was also terminated with an n-GaAs cap grown at T_s = 630ºC. The layers for sample 320GaAs were completed with a 1.0 µm/hr growth rate. The real time growth progression of all the samples was monitored from an in-situ reflection high energy electron diffraction (RHEED), which was recorded through a charge-coupled device (CCD). The CCD was positioned directly in front of the RHEED phosphor screen.

The crystal quality of the samples was obtained using high resolution Shimadzu XRD-7000 X-ray diffractometer. The X-ray source was from a 2.7 kW broad focus Copper (Cu) tube with characteristic wavelengths at 1.540562 Å and 1.54439 Å corresponding to the Cu-$K\alpha_1$ and Cu-$K\alpha_2$ spectral lines, respectively. The scan range was from 2θ = 65º to 2θ = 70º with step size of 0.01º. The measurement time was set to 0.2 seconds. The Raman scattering of the samples was also determined using a µ-Raman spectroscopy in a (100) backscattering geometry. A 514.5 nm Ar^+ laser source was used with the power kept at 60 mW. The laser beam with spot size of 500 nm was focused onto the sample surface through a 100x magnification objective lens. The Raman signal was fiber fed to a Synapse Si CCD detector, which was connected to a Horiba Jobin Yvon iHr 550 imaging spectrometer. The spectrometer resolution was set to < 0.5 cm^{-1}.

The THz time-domain spectroscopy was performed in reflection and transmission excitation geometries [1, 23]. The excitation source was a 800 nm, p-polarized, mode-locked Ti:Sapphire pulsed laser. The pulse width was at 100 fs with 80 MHz repetition rate and with chopping frequency set to 2 kHz. The laser source was split into pump and probe beams incident onto the sample and detector, respectively. There was a mechanical delay stage for the pump beam. In the reflection (transmission) geometry, the pump beam was incident on the sample at 45º (60º)-angle relative to the sample surface. The average pump (probe) power was at 120 mW (5 mW). The detector was a commercial LTG-GaAs dipole PCA with Si lens.

Results And Discussion

A representative RHEED progression during the MBE growth of the GaAs on Si samples is shown in Fig. 3. The passivating layer (oxide) removal has resulted to an RHEED pattern with 2x2 reconstruction, consistent with thermally cleaned Si (100) substrate [24]. Upon deposition of the first LTG-GaAs buffer, spotty features are observed indicative of an island GaAs growth [24, 25]. The spots gradually changed to streaks when T_s is raised for the first annealing. Upon deposition of the second LTG-GaAs, a streaky 1x1 RHEED pattern is observed, conforming with LTG-GaAs deposited on a GaAs substrate [22, 26]. The

second annealing has also resulted to a streaky pattern. The RHEED then exhibited a streaky 2x4 surface reconstruction during the GaAs epitaxial growth, signifying a layer-by-layer GaAs growth [9, 24, 27]. There is no observed amorphous layer transition throughout the growth duration. The two-layered, LTG-GaAs buffer with subsequent in-situ thermal annealing proved effective in addressing the lattice mismatch between the GaAs and Si.

Similarly, the growth method is suitable in managing the thermal expansion coefficient difference between the GaAs and Si. There are no cracks and pinholes on the surface of the GaAs on Si samples as shown in Fig. 4. The surface photographs of the samples, shown in Fig. 4(a), are all specular indicating macroscopically smooth surfaces. However, in contrast with the 320GaAs sample, there are visible mosaic-like features on the top-view scanning electron microscope (SEM) images of the GaAs on Si samples as shown in Fig. 4(b). These features correspond to the antiphase domains (APDs), which are regions formed from APBs [28, 29]. The successful elimination of APBs has been achieved for GaAs grown on misoriented Si (100) substrate [8, 11, 17, 30]. In this work, exactly oriented Si (100) substrates are used, thus the expected appearance of APBs. The average APD sizes for samples 320Si, 520Si and 630Si are approximately 0.8 μm^2, 2.1 μm^2, and 5.3 μm^2, respectively. The sizes are observed to increase with increasing T_s suggesting a reduction in the density of APBs at higher T_s. When GaAs is deposited at higher T_s, the migration length of the Ga and As atoms becomes longer [31, 32]. This is more favorable for Ga-As bonding, hence can reduce the Ga-Ga and As-As bonds that form the APBs. The cross-sectional view SEM images of the samples are shown in Fig. 4(c). The GaAs/Si interface can be clearly seen for the GaAs on Si samples while there is no interface in the 320GaAs sample. There are also some observed growth misorientations in the GaAs epilayer relative to the Si (100) substrate surface for the GaAs on Si samples. The resulting GaAs misorientation is associated with threading dislocations from either twinning features or stacking faults most commonly on (111) or (1-1-1) planes due to the lattice mismatch [6, 7, 30]. Nevertheless, the dislocations are not detrimental on account of the interface being free from cracks and pinholes, and the desired GaAs thickness has been achieved.

Shown in Fig. 5 are the normalized X-ray rocking curves of the samples on (004)-reflection plane. The Cu-$K\alpha_1$ and Cu-$K\alpha_2$ spectral lines from the X-ray source are highly resolved in both the Si (004) and GaAs (004) fundamental diffraction peaks. In consideration thereof, Gaussian curves are fitted to distinguish the Si and GaAs peaks. The Si peak position and its corresponding full width at half maximum (FWHM) are determined to be similar for the GaAs on Si samples. The Si peak position is at 69.236 ± 0.002º with FWHM of 0.460 ± 0.023º. Conversely, summarized in Table 1 are the parameters obtained from the GaAs peak. From the peak position, the calculated lattice constants perpendicular to the (100) surface of both the Si and SI-GaAs substrates collectively deviates by < 0.35% from the ideal GaAs lattice constant of a_0 = 5.6533Å [33]. The small deviation suggests that the GaAs epilayer tends to relax towards a_0 even for the GaAs on Si samples proving the effectiveness of the implemented growth method. Nevertheless, there is a difference in the GaAs FWHM for the GaAs on Si samples. A decreasing trend in the GaAs FWHM is observed as T_s is increased during the deposition of GaAs on Si substrates, which indicates an improvement in the crystal quality [5, 7]. This improvement is in agreement with the increasing APD size

(reduction in APB density) observed from the top-view SEM images of the GaAs on Si samples as T_s is increased. The crystallinity of the grown GaAs on Si samples as observed in the SEM images and X-ray rocking curves is consistent with the measured carrier mobility presented in a previous work [34].

Table 1. The GaAs (004) parameters obtained from the X-ray diffraction.

The values are from the calculated Gaussian curve fitting.

Sample	GaAs (004)		
	Peak Position 2θ (°)	Lattice Constant (Å)	FWHM (°)
320GaAs	66.306 ± 0.005	5.6357 ± 0.0001	0.527 ± 0.012
320Si	66.235 ± 0.004	5.6410 ± 0.0001	0.586 ± 0.010
520Si	66.236 ± 0.005	5.6409 ± 0.0001	0.448 ± 0.008
630Si	66.250 ± 0.005	5.6398 ± 0.0001	0.433 ± 0.009

Shown in Fig. 6 are the Raman spectra of the samples. Two peaks are resolved corresponding to the longitudinal optical (LO) and transverse optical (TO) phonons in GaAs. Summarized in Table 2 are the LO-TO phonon parameters obtained from the Raman spectra fitted with a Lorentzian curve. The separation of the LO and TO phonon peaks for the 320GaAs sample is 25.38 ± 0.59 cm^{-1}. The GaAs on Si samples are characterized by comparable LO-TO peak separations as that of 320GaAs but with higher TO/LO peak intensity ratio. The TO intensity relative to the LO intensity is observed to increase with increasing T_s. The Raman shift on a (100) surface acquired from backscattering geometry theoretically forbids TO mode [35, 36]. The higher TO/LO peak intensity ratio in the GaAs on Si samples relative to 320GaAs is attributed to some misorientation of the GaAs growth relative to the Si (100) substrate surface as seen from the cross-sectional view SEM images. Subsequently, in backscattering geometry, both the TO and LO phonon modes are observable for (111) crystal surfaces [35, 37]. It can be inferred that the GaAs misorientation by threading dislocations propagating towards the surface are most likely to be (111)-oriented and are highly probable if GaAs is grown on Si at higher T_s. On the other hand, there is an apparent broadening in the LO phonon peak of sample 630Si. The broadening of phonon peaks manifest from crystal defects [37, 38]. Considering the reduced APB density, the relatively sharp GaAs (004) X-ray diffraction, and the plausible (111)-oriented threading dislocations, the 630Si sample could have exhibited a comparable LO phonon FWHM relative to the other GaAs on Si samples. The same planar and line defects are also present in samples 320Si and 520Si and are less favorable defect-wise. It can then be surmised that there is an unintentional incorporation of point defects in 630Si within the penetration depth (~ 124 nm) of the laser source that may have caused the broadening [39]. This could also be the reason behind the intensity decrease of the same LO phonon peak. The validation on the possible point defects incorporation, however, is beyond the scope of this work.

Table 2. The LO-TO phonon parameters obtained from the Raman spectra.

The values are from the calculated Lorentzian curve fitting.

Sample	LO-TO Peak Separation (cm^{-1})	TO/LO Peak Intensity Ratio	LO FWHM (cm^{-1})
320GaAs	25.38 ± 0.59	0.09	8.49 ± 0.09
320Si	23.63 ± 0.32	0.16	11.58 ± 0.10
520Si	25.27 ± 0.15	0.21	9.32 ± 0.09
630Si	23.51 ± 0.23	0.45	16.92 ± 0.25

The THz emission of the samples in reflection and transmission excitation geometries are shown in Figs. 7 and 8. The GaAs on Si samples grown at higher T_s emerge as promising THz emitters. Summarized in Table 3 are the corresponding peak-to-peak THz emission intensities. In reflection geometry, 320Si has exhibited a 34% reduction in the THz emission intensity relative to 320GaAs. This is attributed to the lower crystallinity of 320Si than 320GaAs as confirmed from X-ray diffraction. Sample 320Si is also observed to have the highest APB density from the SEM images. Interestingly, even with the presence of APBs and threading dislocations, sample 520Si has exhibited an 89% increase in the THz emission intensity relative to 320GaAs while the THz emission intensity of 630Si is comparable with 320GaAs. It can be inferred that the THz emission in GaAs on Si samples is not completely limited by the presence of APBs, threading dislocations and thus crystallinity. Within the ~ 1 μm penetration depth of the 800 nm excitation source, the presence of structural defects in the GaAs epilayer is favorable in increasing the surface electric field thus resulting in an enhanced THz emission for GaAs on Si grown at T_s > 320ºC. Similar surface-field induced THz emission enhancement has been observed for GaAs microstructures and As-rich GaAs [14, 16]. Nevertheless, the results suggest that there exists an optimal T_s at which the THz emission is most efficient for GaAs on Si samples. It should be noted that for LTG-GaAs on SI-GaAs, high photoexcited carrier mobility, due to high crystallinity, and the presence of few As clusters in the LTG-GaAs are two important factors for intense THz generation [16]. In a previous study, 630Si has been shown to have higher carrier mobility than 520Si attributed to the higher crystallinity of 630Si [34], which is consistent with the SEM images and Xray diffraction results presented in this work. Despite the lower crystal quality, 520Si exhibits a higher THz emission indicating that the enhancement is not solely dependent on carrier mobility but also on the optimal presence of structural defects such as the APBs.

Table 3. Peak-to-peak THz emission intensities in reflection and transmission excitation geometries.

Sample	Reflection (Ref) Peak-to-Peak Intensity (nA)	Transmission (Trans) Peak-to-Peak Intensity (nA)	Trans/Ref Intensity Ratio
320GaAs	0.907	0.382	0.42
320Si	0.603	0.318	0.53
520Si	1.718	1.361	0.79
630Si	0.903	0.685	0.76

In transmission geometry, there is a general decrease in the THz emission intensity of the samples than in reflection geometry due to absorption losses. The transmission over reflection THz intensity ratios of the samples are summarized in Table 3. The GaAs on Si samples have higher intensity ratios than sample 320GaAs. These results show that GaAs grown on a Si substrate have less absorption losses than GaAs grown on an SI-GaAs substrate. Correspondingly, the absorption coefficient below 2 THz of Si is less than that of GaAs [19]. Therefore, it is desirable to use Si substrates in THz transmission geometry despite the absorption losses. With regards to the THz emission intensity, the same trend is observed for the GaAs on Si samples in transmission geometry. Sample 520Si still exhibited the highest THz emission intensity followed by 630Si and then 320Si.

Shown in the inset of Figs. 7 and 8 are the corresponding power spectra of the THz waveforms. The frequency bandwidth in reflection geometry of all the samples is ~ 0.6 THz while it is ~ 0.4 THz in transmission geometry. There is an apparent THz absorption around the frequency range of 0.2–0.6 THz in the transmission geometry for all samples. For 320GaAs, this is expected since the GaAs substrate (resistivity ~ 10.0 MΩ.cm) has significant absorption in 0.2-2.0 THz [19]. For the GaAs on Si samples, the THz absorption is attributed to the low resistivity of the Si substrate (resistivity ~ 1.0 KΩ.cm) resulting to the presence of carriers from residual impurities [18–20]. At high resistivity (> 10.0 KΩ.cm), Si substrate generally is more transparent in the THz frequency region [18–20].

Summary And Conclusions

In this work, the THz emission of GaAs on Si thin films exhibiting structural defects in the GaAs epilayer have been investigated in both reflection and transmission THz time-domain excitation geometries. The GaAs epilayers are grown by MBE on exactly oriented Si (100) substrates at different growth temperatures, T_S = 320°C, 520°C and 630°C. The growth schematic involves the deposition of two LTG-GaAs buffers subsequently annealed at T_S = 600°C. The epitaxial growth progression has been monitored by RHEED, which confirms the layer-by-layer growth mode of the GaAs on Si. The crystallinity of the thin films has been shown to improve with increasing T_S from X-ray diffraction analysis. Nevertheless, there still are the presence of APBs and threading dislocations as identified through SEM and Raman

spectroscopy. The density of APBs decreases with increasing T_s while the threading dislocations with (111) orientation becomes more probable at high T_s.

Accordingly, in reflection geometry, there is a 34% reduction in the THz emission of the GaAs on Si sample grown at T_s = 320ºC relative to its GaAs on SI-GaAs counterpart. The low crystallinity of GaAs on Si at T_s = 320ºC makes it an inferior THz emitter. However, at higher T_s, GaAs on Si samples emerge as promising THz emitters. The most intense THz emission is observed in GaAs on Si grown at T_s = 520ºC. In transmission geometry, the GaAs on Si sample is also more desirable than the GaAs on SI-GaAs sample owing to the higher transparency of the Si substrate in the THz frequency.

It can be concluded that even with structural defects, GaAs on Si is a more effective material system over LTG-GaAs homostructure in the generation of THz radiation in both reflection and transmission excitation geometries. An intense THz emission has been observed despite the presence of APBs and threading dislocations. Consequently, there exists an optimal T_s for GaAs on Si where THz emission is most intense. Results have shown that this T_s does not necessarily correspond to the GaAs on Si with the highest crystallinity. By simply changing T_s, the implemented growth method demonstrates an effective way to regulate the incorporation of structural defects in GaAs on Si that is advantageous to the THz emission enhancement in both excitation geometries. However, an extensive analysis on the structural defects that exist within the GaAs on Si thin films is recommended to correlate the defect density with the surface field-induced THz emission enhancement. These findings are particularly important in the growth design and fabrication of GaAs on Si material system for THz photoconductive antenna emitter devices.

Declarations

Funding/Acknowledgement

E. A. Prieto, A. Somintac, E. Estacio and A. Salvador acknowledge the Office of the Chancellor of the University of the Philippines Diliman, through the Office of the Vice Chancellor for Research and Development, for funding support through the Outright Research Grant. The authors also acknowledge the assistance of R. Jagus and K. Patrocenio in maintaining the molecular beam epitaxy facility of the National Institute of Physics, University of the Philippines Diliman.

Conflicts of interest/Competing interests

The authors declare no known conflicts of interest or competing interests that are directly or indirectly related to the work.

Availability of data and material

All data are available upon reasonable request from the authors.

Code availability

Not applicable.

Authors' contributions

The conceptualization, analysis, investigation, and validation of the work are credited to KC Gonzales, EA Prieto, E Estacio, and A Salvador. The data acquisition and methodology are performed by KC Gonzales, EA Prieto, GA Catindig, A De Los Reyes, MA Faustino, MA Tumanguil-Quitoras, HA Husay, and JD Vasquez. The manuscript writing is done by KC Gonzales, EA Prieto, GA Catindig, E Estacio, and A Salvador. The supervision, resources, and funding acquisition are through the efforts of EA Prieto, A Somintac, E Estacio, and A Salvador. All authors read and approved the final manuscript.

Ethics approval

The research does not involve human participants and/or animals.

Consent to participate

Not applicable.

Consent for publication

The publication has been approved by all authors.

References

1. T. Yoshioka, S. Takatori, P.H. Minh, M. Catadal-Raduban, T. Nakazato, T. Shimizu, N. Sarakura, E. Estacio, J.V. Misa, R. Jaculbia, M. Defensor, A. Somintac, A. Salvador, Terahertz Emission from GaAs Films on Si (100) and Si (111) Substrates Grown by Molecular Beam Epitaxy, Infrared Milli Terahertz Waves 32 (2011)
2. E. Estacio, S. Takatori, M.H. Pham, T. Yoshioka, T. Nakazato, M. Cadatal-Raduban, T. Shimizu, N. Sarukura, M. Hangyo, C.T. Que, M. Tani, T. Edamura, M. Nakajima, J.V. Misa, R. Jaculbia, A. Somintac, A. Salvador, Intense terahertz emission from undoped GaAs/n-type GaAs and InAs/AlSb structures grown on Si substrates in the transmission-geometry excitation. Appl. Phys. B Lasers Opt. **103**, 825–829 (2011)
3. J. Klier, G. Torosyan, N.S. Schreiner, D. Molter, F. Ellrich, W. Zouaghi, E. Peytavit, J.-f. Lampin, R. Beigang, J. Jonuscheit, G.V. Freymann, Influence of Substrate Material on Radiation Characteristics of THz Photoconductive Emitters, Int. J. Antennas Propag. 2015 (2015)
4. R. Fischer, N. Chand, W. Kopp, H. Morkoç, L.P. Erickson, R. Youngman, GaAs bipolar transistors grown on (100) Si substrates by molecular beam epitaxy. Appl. Phys. Lett. **47**, 397–399 (1985)
5. D.A. Neumann, H. Zabel, R. Fischer, H. Morkoç, Structural properties of GaAs on (001) oriented Si and Ge substrates. J. Appl. Phys. **61**, 1023–1029 (1987)

6. S.M. Koch, S.J. Rosner, R. Hull, G.W. Yoffe, J.S. Harris, The growth of GaAs on Si by MBE. J. Cryst. Growth **81**, 205–213 (1987)
7. J.W. Lee, H. Shichijo, H.L. Tsai, R.J. Matyi, Defect reduction by thermal annealing of GaAs layers grown by molecular beam epitaxy on Si substrates. Appl. Phys. Lett. **50**, 31–33 (1987)
8. S.F. Fang, K. Adomi, S. Iyer, H. Morkoç, H. Zabel, C. Choi, N. Otsuka, Gallium arsenide and other compound semiconductors on silicon, J. Appl. Phys. 68 (1990)
9. P. Taylor, W. Jesser, J. Benson, M. Martinka, J. Dinan, J. Bradshaw, M. Lara-Taysing, R. Leavitt, G. Simonis, W. Chang, W. Clark III, K. Bertness, Optoelectronic device performance on reduced threading disloctation density Gaas/Si. J. Appl. Phys. **89**, 4365–4375 (2001)
10. W. Stolz, F.E.G. Guimaraes, K. Ploog, Optical and structural properties of GaAs grown on (100) Si by molecular beam epitaxy. J. Appl. Phys. **63**, 492–499 (1987)
11. Y.B. Bolkhovityanov, O.P. Pchelyakov, GaAs epitaxy on Si substrates: Modern status of research and engineering. Phys. Usp. **51**, 437–456 (2008)
12. Y. Buzynin, V. Shengurov, B. Zvonkov, A. Buzynin, S. Denisov, N. Baidus, M. Drozdov, D. Pavlov, P. Yunin, GaAs/Ge/Si epitaxial substrates: Development and characteristics. AIP Adv. **7**, 1–7 (2017)
13. C. Kang, J.W. Leem, I. Maeng, T.H. Kim, J.S. Lee, J.S. Yu, C.-S. Kee, Strong emission of terahertz radiation from nanostructured Ge surfaces. Appl. Phys. Lett. **106**, 261106 (2015)
14. I. Maeng, G. Lee, C. Kang, G.W. Ju, K. Park, S.B. Son, Y.T. Lee, C.S. Kee, Strong emission of THz radiation from GaAs microstructures on Si, AIP Adv. 8 (2018)
15. M. Tani, S. Matsuura, K. Sakai, S. Nakashima, Emission characteristics of photoconductive antennas based on low-temperature grown GaAs and semi-insulating GaAs. Appl. Opt. **36**, 7853–7859 (1997)
16. Y. Kamo, S. Kitazawa, S. Ohshima, Y. Hosoda, Highly efficient photoconductive antennas using optimum low-temperature-grown GaAs layers and Si substrates. Jpn. J. Appl. Phys. **53**, 032201 (2014)
17. R. Alcotte, M. Martin, J. Moeyaert, R. Cipro, S. David, F. Bassani, F. Ducroquet, Y. Bogumilowicz, E. Sanchez, Z. Ye, X.Y. Bao, J.B. Pin, T. Baron, Epitaxial growth of antiphase boundary free GaAs layer on 300 mm Si (001) substrate by metalorganic chemical vapour deposition with high mobility, APL Mater. 4 (2016)
18. T. Ohba, S. Ikawa, Far-infrared absorption of silicon crystals. J. Appl. Phys. **64**, 4141–4143 (1988)
19. D. Grischkowsky, S. Keiding, M. van Exter, C. Fattinger, Far-infrared time-domain spectroscopy with terahertz beams of dielectrics and semiconductors. J. Opt. Soc. Am. B **7**, 2006–2015 (1990)
20. J. Dai, J. Zhang, W. Zhang, D. Grischkowsky, Terahertz time-domain spectroscopy characterization of the far-infrared absorption and index of refraction of high-resistivity, float-zone silicon. J. Opt. Soc. Am. B **21**, 1379–1386 (2004)
21. D.C. Look, Z.-Q. Fang, J.R. Sizelove, C. E. Stutz, New As Ga Related Center in GaAs. Phys. Rev. Lett. **70**, 465–468 (1993)

22. M. Missous, Stoichiometric low temperature (SLT) GaAs and Al-GaAs grown by molecular beam epitaxy. Microelectron. J. **27**, 393–409 (1996)
23. E.A.P. Prieto, S.A.B. Vizcara, L.P. Lopez, J.D.E. Vasquez, M.H.M. Balgos, D. Hashizume, N. Hayazawa, Y. Kim, M. Tani, A.S. Somintac, A.A. Salvador, E.S. Estacio, Intense THz emission in high quality MBE-grown GaAs film with a thin n-doped buffer. Opt. Mater. Express **8**, 1463–1471 (2018)
24. S. Nishi, H. Inomata, M. Akiyama, K. Kaminishi, Growth of single domain GaAs on 2-inch Si (100) substrate by molecular beam epitaxy. Jpn. J. Appl. Phys. **24**, L391–L393 (1985)
25. K. Asai, K. Kamei, H. Katahama, Lattice relaxation of GaAs islands grown on Si (100) substrate. Appl. Phys. Lett. **71**, 701–703 (1997)
26. E.A.P. Prieto, S.A.B. Vizcara, A.S. Somintac, A.A. Salvador, E.S. Estacio, C.T. Que, K. Yamamoto, M. Tani, Terahertz emission enhancement in low-temperature-grown GaAs with an n-GaAs buffer in reflection and transmission excitation geometries. J. Opt. Soc. Am. B **31**, 291–295 (2014)
27. K. Sprung, K. Wilke, G. Heymann, J. Varrio, M. Pessa, GaAs single domain growth on exact (100) Si substrate. Appl. Phys. Lett. **62**, 2711–2712 (1993)
28. I. Németh, B. Kunert, W. Stolz, K. Volz, Heteroepitaxy of GaP on Si: Correlation of morphology, anti-phase-domain structure and MOVPE growth conditions. J. Crys. Growth **310**, 1595–1601 (2008)
29. O. Rubel, S. Baranovskii, Formation energies of antiphase boundaries in GaAs and GaP: An ab initio study. Int. J. Mol. Sci. **10**, 5104–5114 (2009)
30. J.W. Lee, H.L. Tsai, Crystal orientations and defect structures of GaAs layers grown on misoriented Si substrates by molecular-beam epitaxy. Journal of Vacuum Science & Technology B: Microelectronics Processing and Phenomena **5**, 819–821 (1987)
31. R. Farrow, Molecular Beam Epitaxy: Applications to key materials, materials science and process technology series: Electronic materials and process technology, Elsevier Science, 2012 URL: https://books.google.com.ph/books?id=EuI6WV8NlnkC
32. M. Henini, Molecular Beam Epitaxy: From Research to Mass Production, Elsevier Science, 2018 URL: https://books.google.com.ph/books?id=sXhiDwAAQBAJ
33. M. Levinshtein, Handbook Series on Semiconductor Parameters, number v.1 in Handbook series on semiconductor parameters, World Scientific, 1997. URL: https://books.google.com.ph/books?id=MSoNFpljBIEC
34. J. Afalla, K.C. Gonzales, E.A. Prieto, G. Catindig, J.D. Vasquez, H.A. Husay, M.A. Tumanguil-Quitoras, J. Muldera, H. Kitahara, A. Somintac, A. Salvador, E. Estacio, M. Tani, Photoconductivity, carrier lifetime and mobility evaluation of GaAs films on Si (100) using optical pump terahertz probe measurements. Semicond. Sci. Technol. **34**, 035031 (2019)
35. R. Loudon, The raman effect in crystals. Adv. in Phys. **13**, 423–482 (1964)
36. B. Prévot, J.Wagner, Raman characterization of semiconducting materials and related structures. Prog. Cryst. Growth Charact. Mater. **22**, 245–319 (1991)

37. G. Abstreiter, E. Bauser, A. Fischer, K. Ploog, Raman spectroscopy - A versatile tool for characterization of thin films and heterostructures of GaAs and Al_xGa_{1-x} As. Appl. Phys. **16**, 345–352 (1978)
38. S. Nakashima, Y. Nakatake, Y. Ishida, T. Talkahashi, H. Okumura, Detection of defects in SiC crystalline films by raman scattering. Physica B **308–310**, 684–686 (2001)
39. C. Kranert, R. Schmidt-Grund, M. Grundmann, Surface- and point defect-related Raman scattering in wurtzite semiconductors excited above the band gap. New J. Phys. **15**, 113048 (2013)

Figures

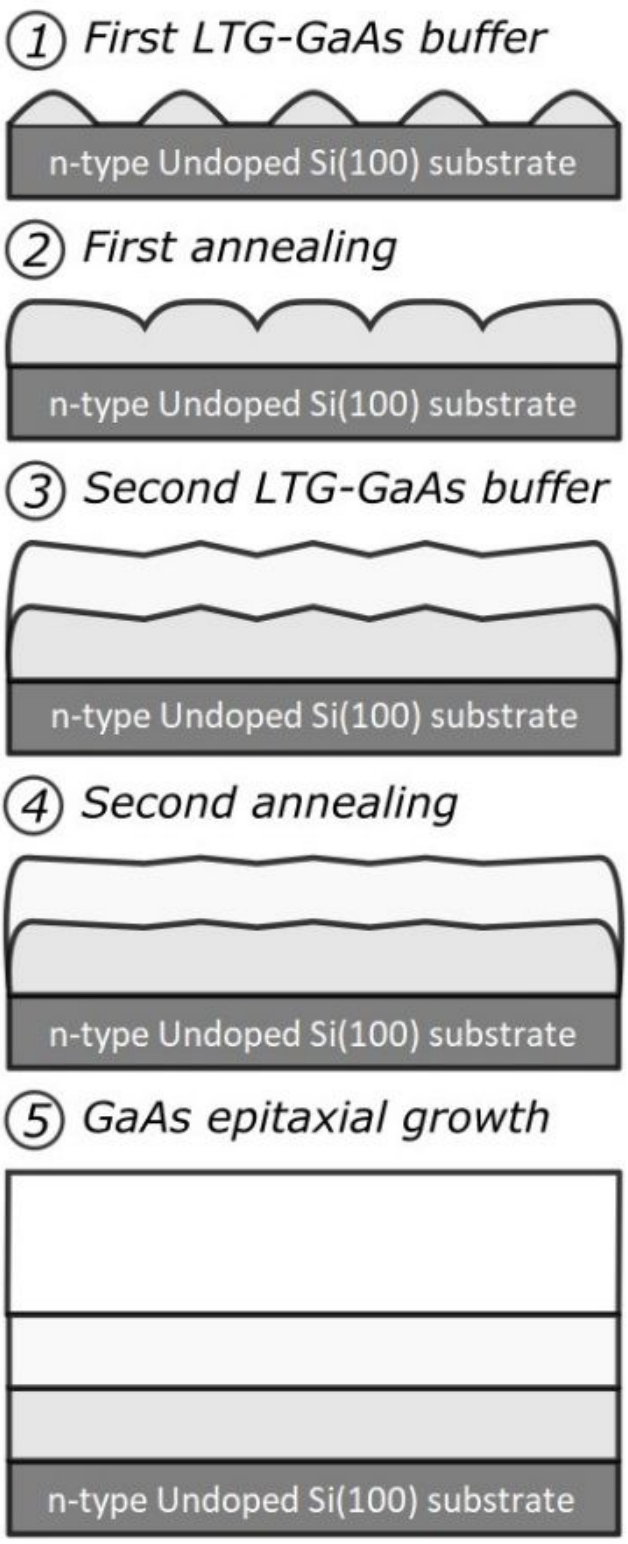

Figure 1

Schematic of the growth method implemented for the deposition of GaAs on n-type undoped Si (100) substrate.

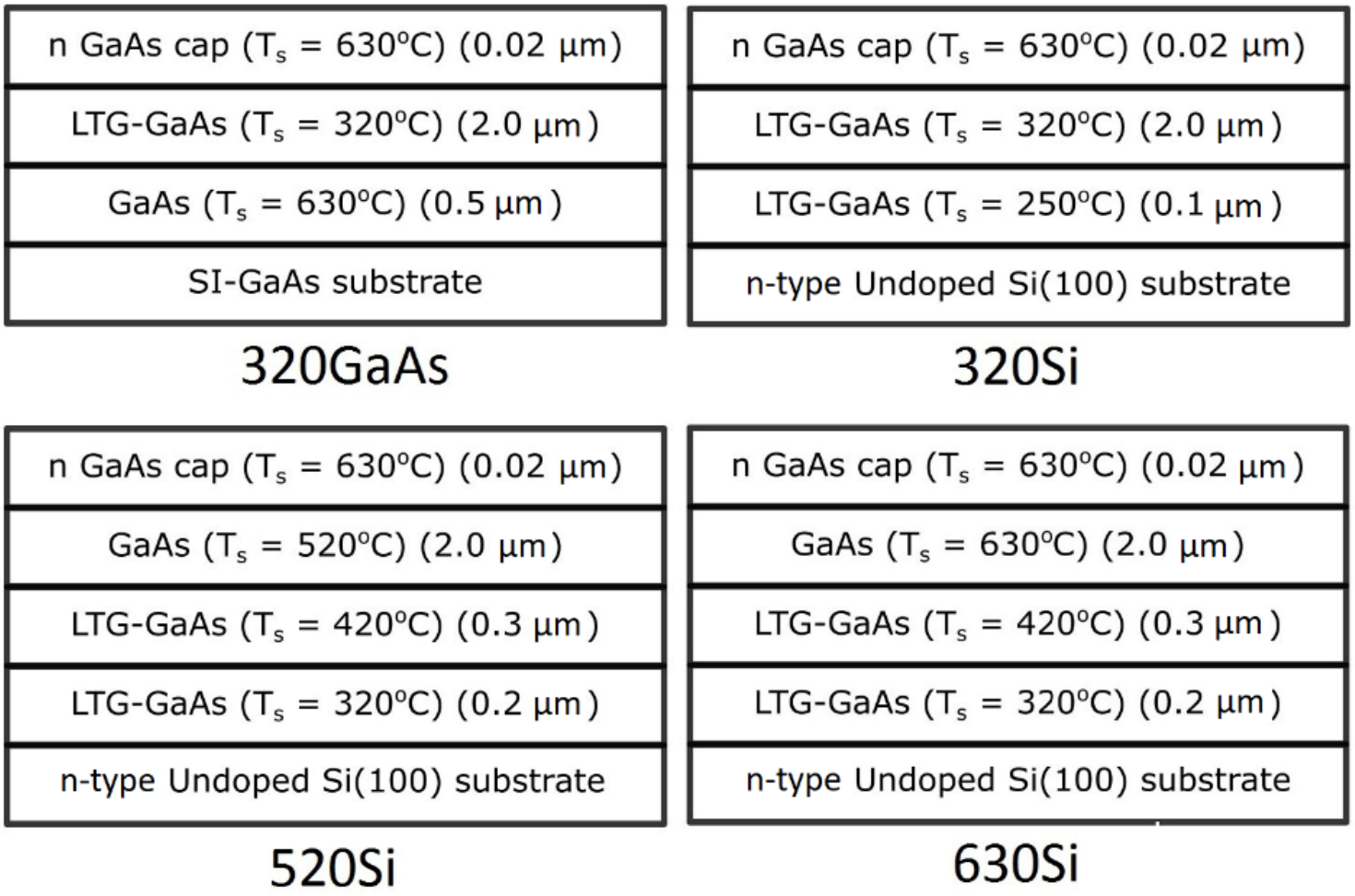

Figure 2

Growth schematic of the MBE-grown samples.

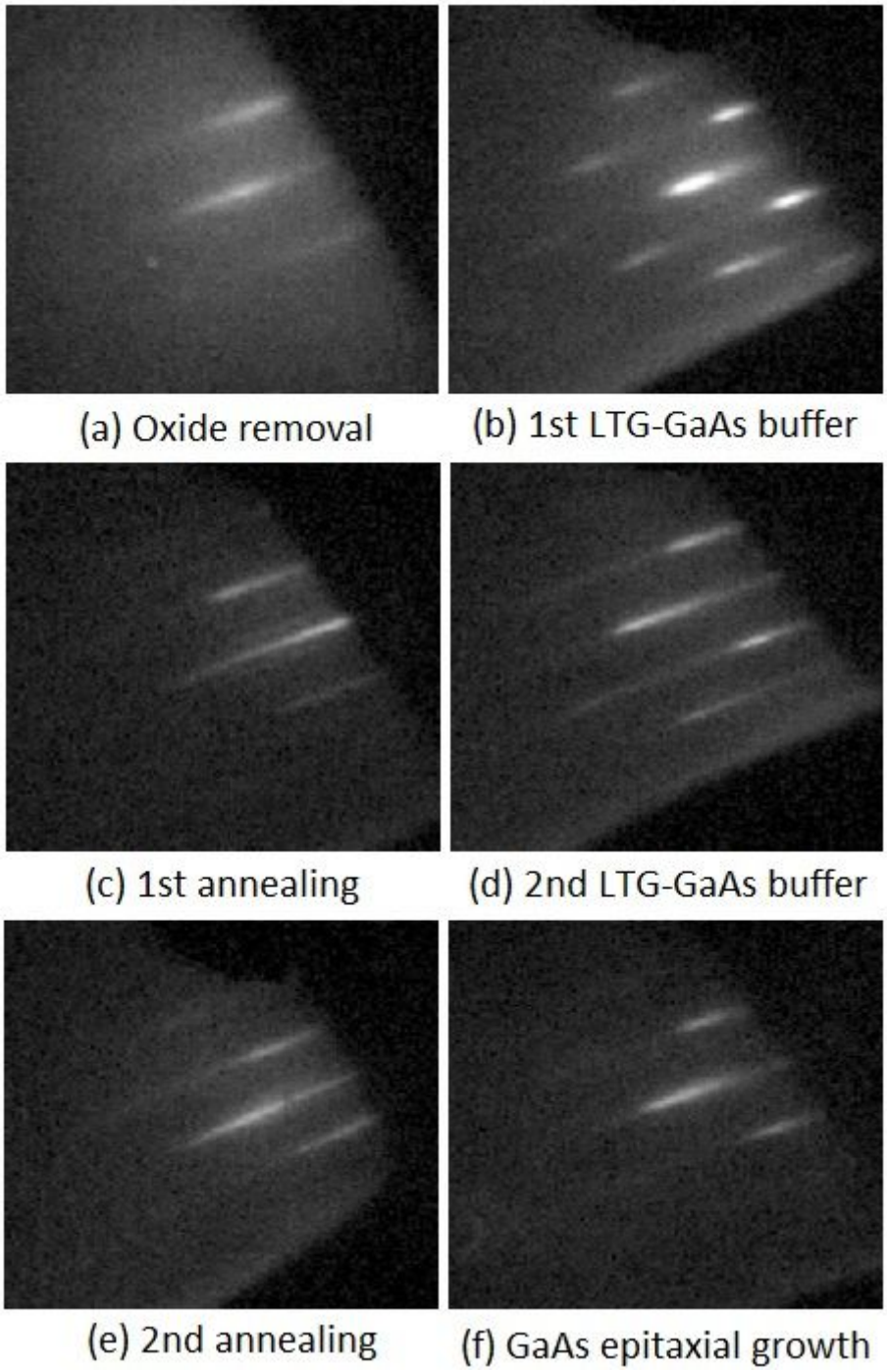

Figure 3

Representative RHEED progression during the MBE growth of the GaAs on Si samples.

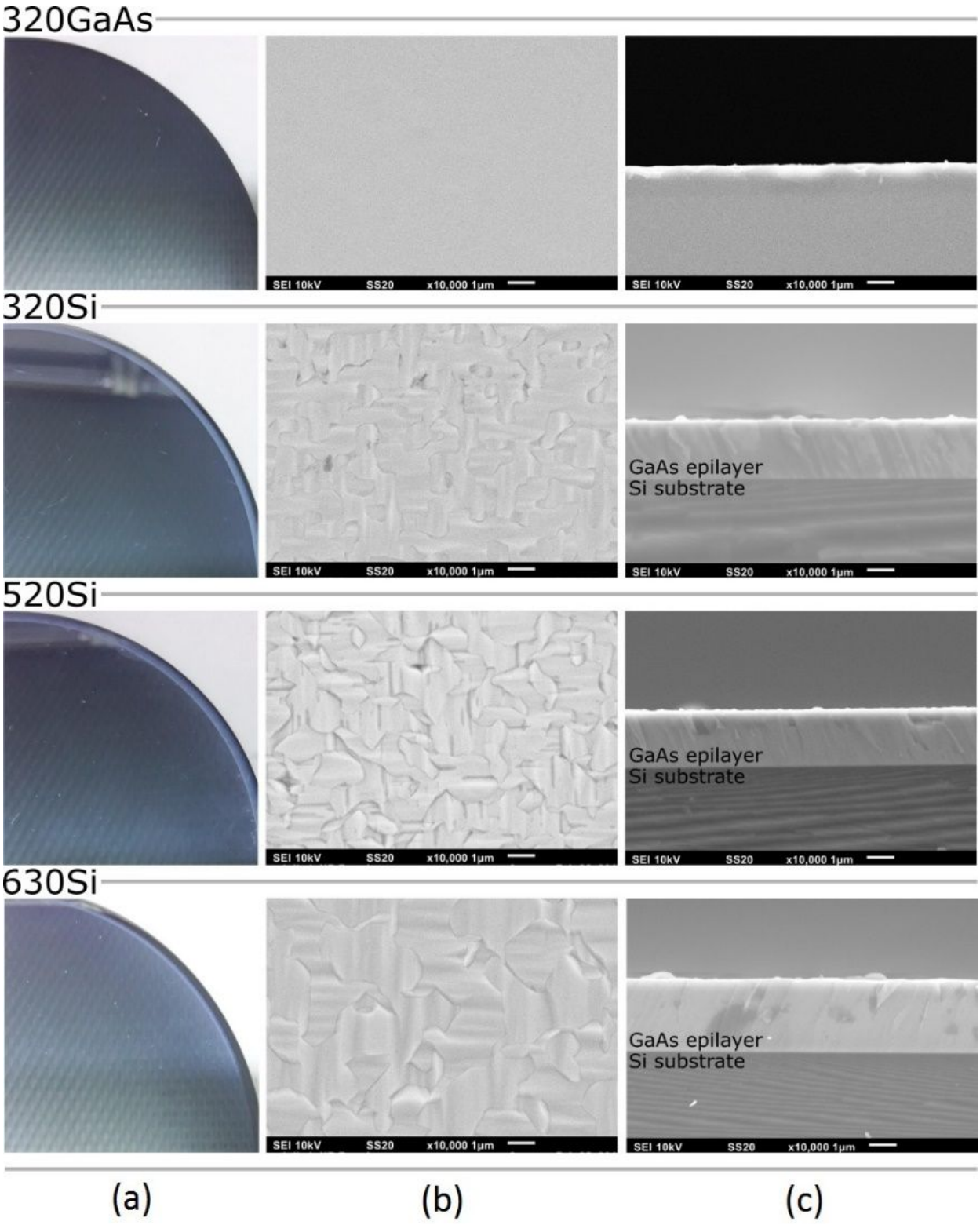

Figure 4

(a) Surface photographs of the samples with the (b) top-view and (c) cross-sectional view SEM images taken at 10,000x magnification. All samples have specular surfaces, reflecting the mesh ceiling and fluorescent lamp of the fumehood where the surface photagraphs are taken. The APDs and the GaAs/Si interface are visible in the top-view and cross-sectional view SEM images, respectively, of the GaAs on Si samples.

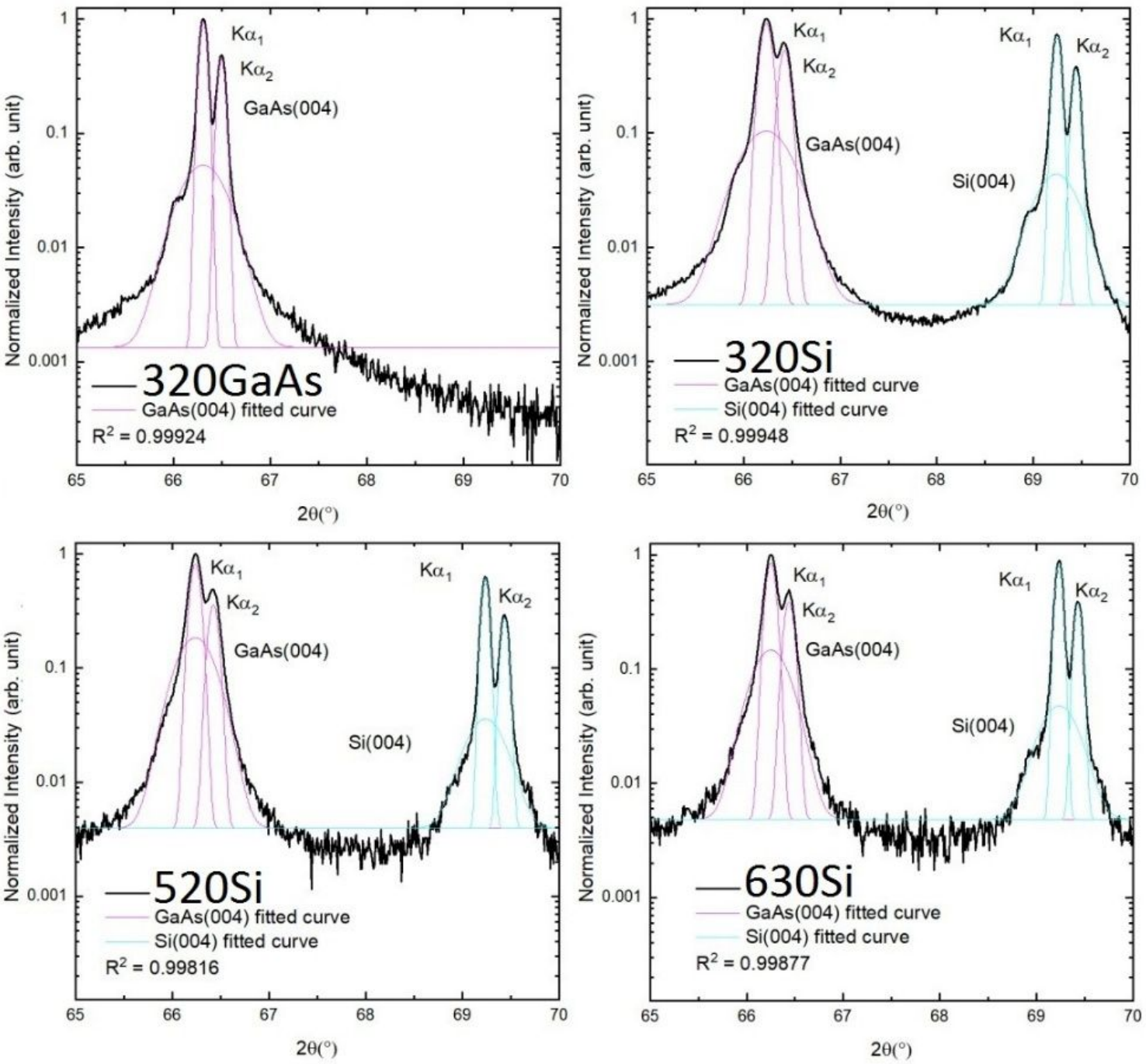

Figure 5

Normalized X-ray diffraction of the samples on (004)-reflection plane with the corresponding Gaussian fitted curves. The two highly resolved peaks correspond to the Cu-Kα1 and Cu-Kα2 spectral lines of the X-ray source. The shoulder peaks are associated with the GaAs and the Si fundamental (004) diffraction peaks.

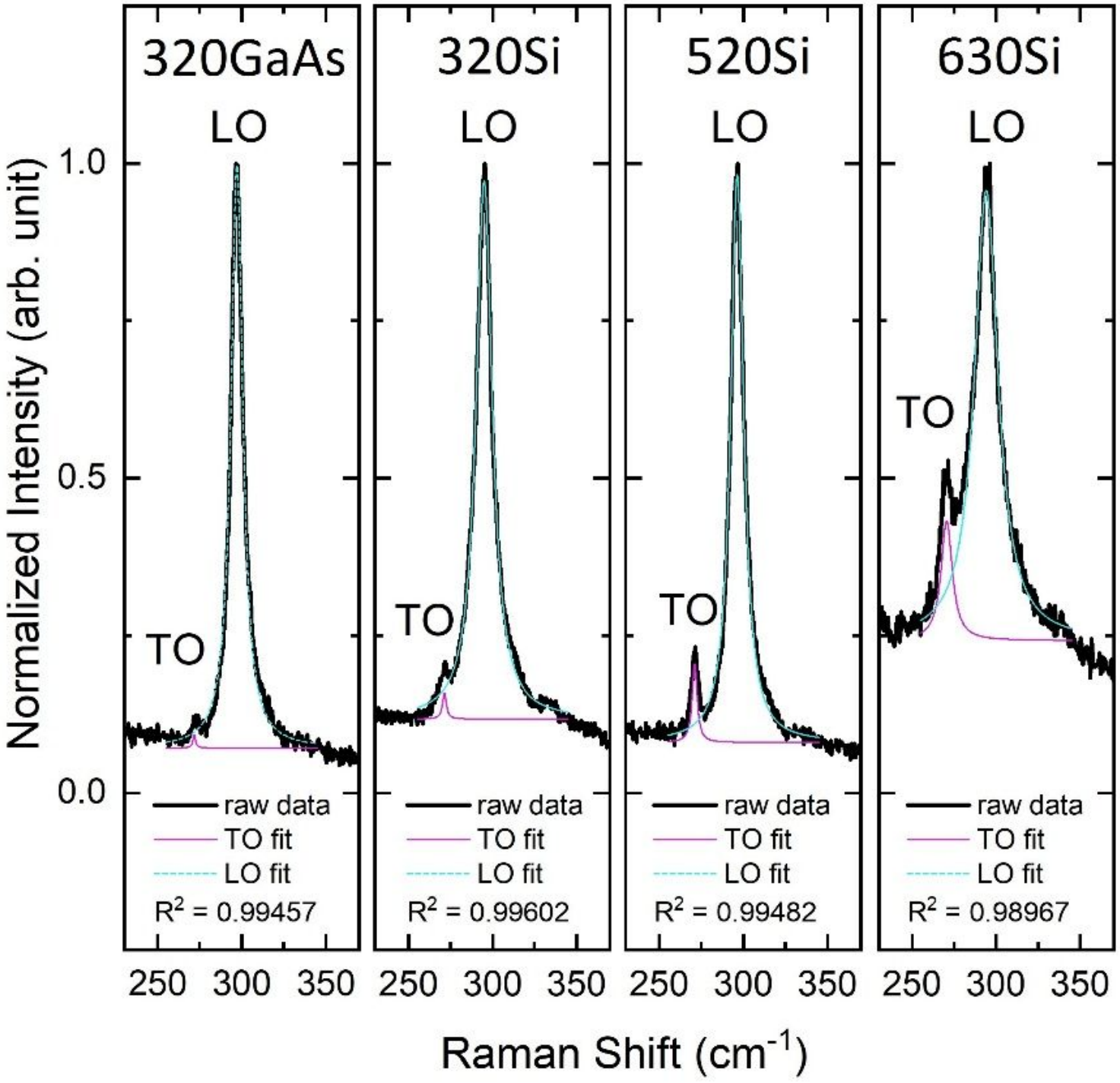

Figure 6

Normalized Raman spectra of the samples with the corresponding Lorenztian fitted curves. The two highly resolved peaks correspond to the LO and TO phonon peaks in GaAs.

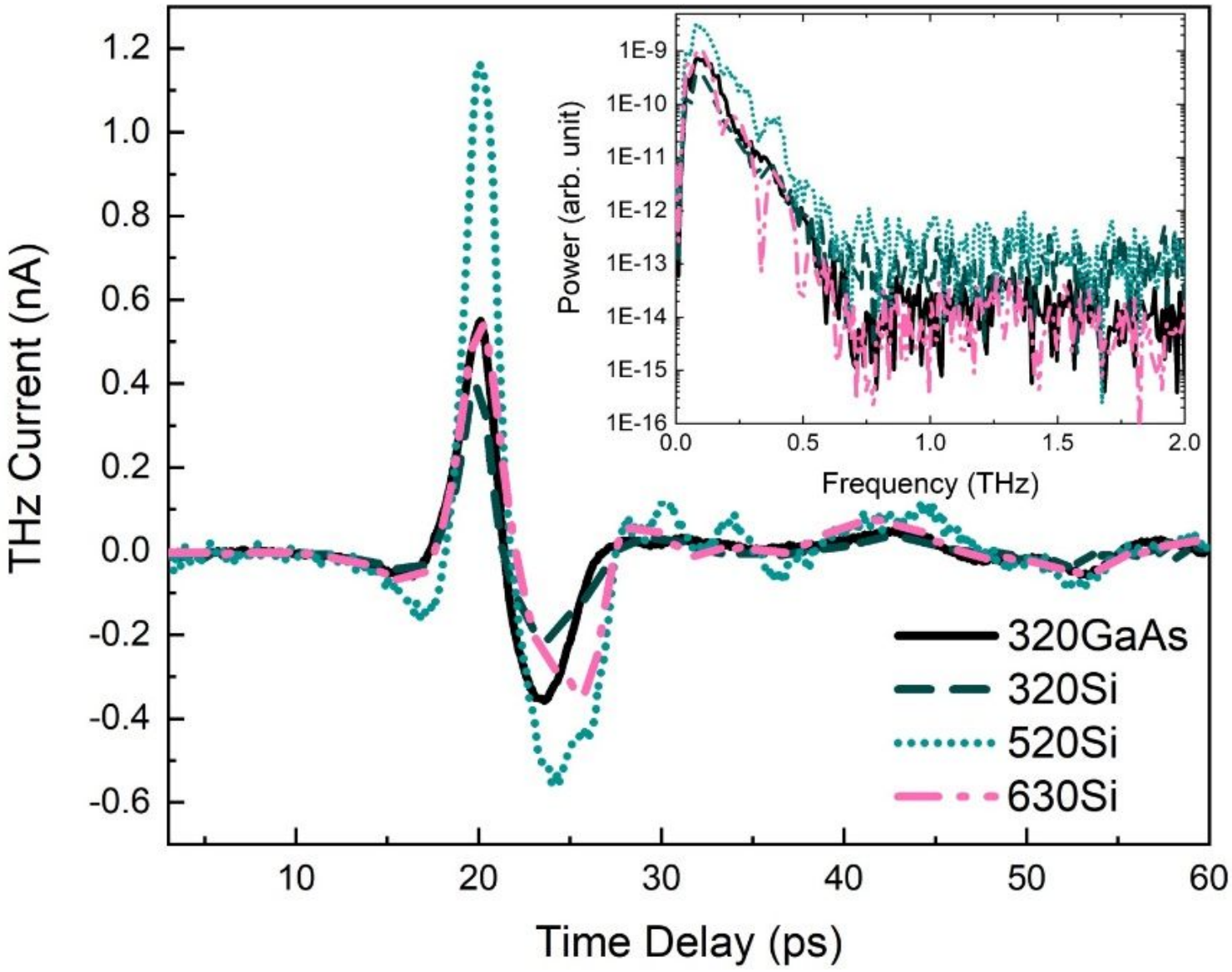

Figure 7

THz emission spectra of the samples in reflection geometry. The inset shows the corresponding power spectra of the THz waveforms.

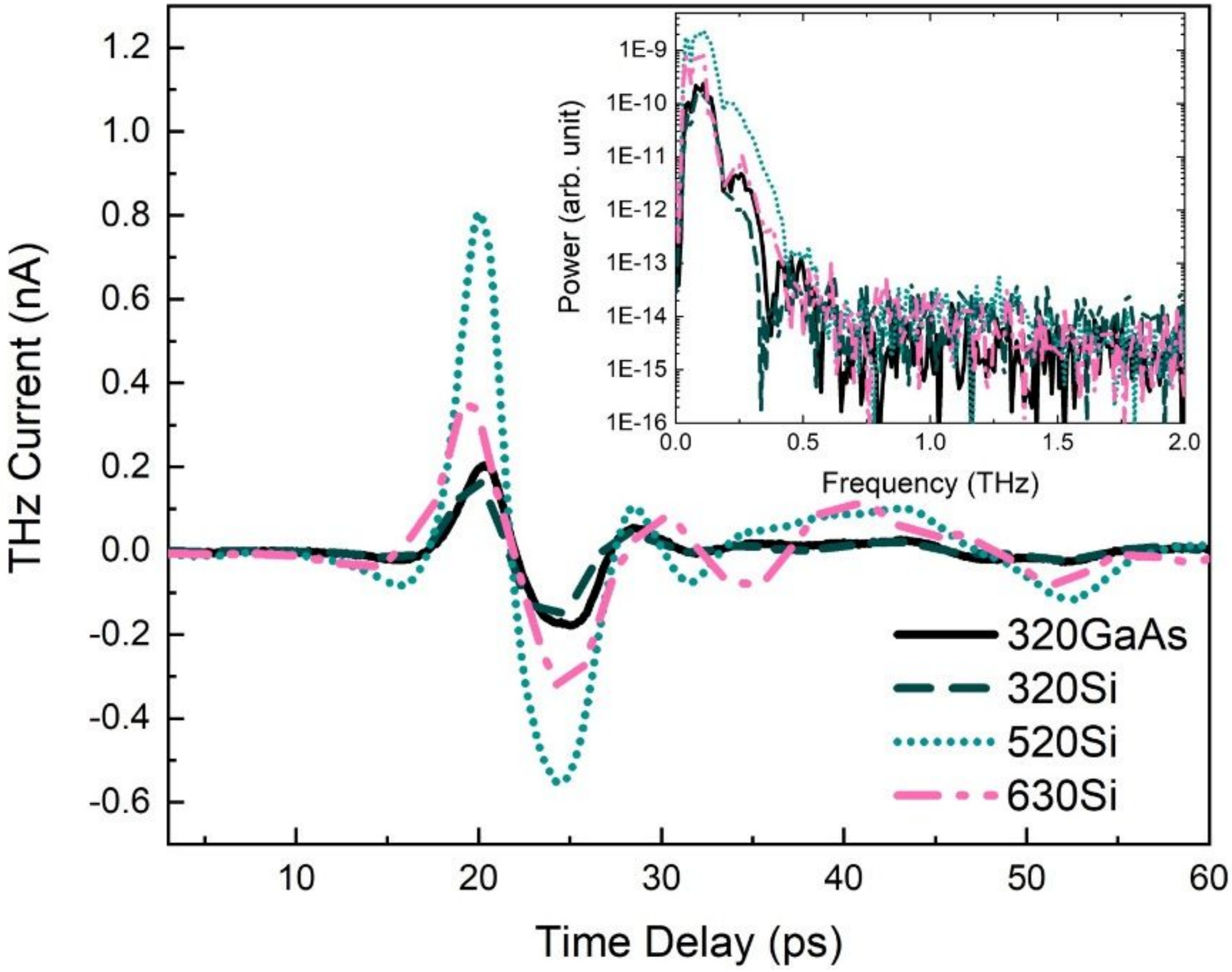

Figure 8

THz emission spectra of the samples in transmission geometry. The inset shows the corresponding power spectra of the THz waveforms.